



HAL
open science

Temperature dependence of coercivity and magnetic relaxation in a Mn–Al–C permanent magnet

Alexandre Pasko, Alexis Pecheux, Muriel Tyrman, Loïc Perrière, Ivan Guillot, Victor Etgens, Martino Lobue, Frédéric Mazaleyrat

► **To cite this version:**

Alexandre Pasko, Alexis Pecheux, Muriel Tyrman, Loïc Perrière, Ivan Guillot, et al.. Temperature dependence of coercivity and magnetic relaxation in a Mn–Al–C permanent magnet. IEEE Transactions on Magnetics, 2021, 10.1109/TMAG.2020.3014741 . hal-02937604

HAL Id: hal-02937604

<https://hal.science/hal-02937604>

Submitted on 14 Sep 2020

HAL is a multi-disciplinary open access archive for the deposit and dissemination of scientific research documents, whether they are published or not. The documents may come from teaching and research institutions in France or abroad, or from public or private research centers.

L'archive ouverte pluridisciplinaire **HAL**, est destinée au dépôt et à la diffusion de documents scientifiques de niveau recherche, publiés ou non, émanant des établissements d'enseignement et de recherche français ou étrangers, des laboratoires publics ou privés.

Temperature dependence of coercivity and magnetic relaxation in a Mn–Al–C permanent magnet

Alexandre Pasko¹, Alexis Pecheux^{1,2}, Muriel Tyrman^{1,3}, Loïc Perrière³,
 Ivan Guillot³, Victor Etgens^{1,4}, Martino LoBue¹, and Frédéric Mazaleyrat¹
¹SATIE, École Normale Supérieure Paris-Saclay, CNRS, 91190 Gif-sur-Yvette, France
²École Normale Supérieure de Rennes, 35170 Bruz, France
³Institut de Chimie et des Matériaux Paris-Est, CNRS, UPEC, 94320 Thiais, France
⁴Synchrotron SOLEIL, 91192 Gif-sur-Yvette Cedex, France

The kinetics of magnetization reversal in a rare-earth-free Mn–Al–C permanent magnet is reported. The L1₀-phase material was prepared using a combination of the melt spinning and spark plasma sintering techniques and characterized with a vibrating sample magnetometer. Magnetic relaxation and susceptibility experiments were performed. Magnetic viscosity, fluctuation field and activation volume were measured in a wide temperature range. These data were used to analyze the magnetization reversal and temperature dependence of the coercive field. The thermally activated mechanism of the reversed nucleus formation was confirmed for the intermediate temperatures. The role of wall thickness and crystallite size as additional characteristic lengths in magnetic domain nucleation is discussed.

Index Terms—Activation volume, coercive field, magnetic viscosity, permanent magnets.

I. INTRODUCTION

THE world market of permanent magnets has been dominated by two groups of optimized materials: high-performance Nd–Fe–B alloys and low-cost hexaferrites. Meanwhile, stimulated by significant changes in price and availability of critical minerals, a third way is gradually emerging: the rare-earth-free hard magnets with intermediate physical properties satisfying the application requirements [1], [2], [3]. A promising candidate for this category (to be used, for example, in the automotive industry) is the Mn–Al system with its ferromagnetic τ -phase which crystallizes in a L1₀ structure [4], [5]. However, in spite of a significant anisotropy field, the values of magnetic coercivity reported so far in Mn–Al-based alloys are relatively low [6], [7], [8]. The difficulty in keeping the coercivity high seems to reside in the particular microstructure (grains, twins) formed in the material as a result of the structural transformations giving rise to the metastable τ -phase. Therefore, further investigations of hysteretic properties of the domain structure are of great interest.

In this paper, we studied the magnetization kinetics in a Mn₅₄Al₄₄C₂ permanent magnet. The work involved a comprehensive magnetic characterization of the material. First, the temperature dependence of the coercive field was investigated. Next, magnetic viscosity experiments were performed in order to observe the effect of thermally activated processes. To estimate the fluctuation field and activation volume of the magnetization reversal, the irreversible susceptibility at the same values of applied field and temperature were also determined. Finally, the obtained experimental data were analyzed in the framework of a model of thermally activated nucleation.

II. EXPERIMENTAL

A ternary alloy of nominal composition Mn₅₄Al₄₄C₂ was produced from high-purity (better than 99.9%) metals by induction melting in a water-cooled copper crucible (in semi-levitation). Carbon was added in the form of Mn₂₃C₆ compound [9]. The carbon content in the cast alloy determined by a combustion analysis was 1.9%. After the surface cleaning, the ingot was remelted in a quartz crucible and rapidly solidified on a copper wheel rotating at a linear speed of 20 m·s⁻¹. The precursor ϵ -phase melt-spun ribbons were subsequently ground with a cryogenic mechanical milling. The obtained powder was compacted in a tungsten carbide mold and sintered in a Syntex Dr. Sinter Lab 515S spark plasma sintering (SPS) setup with an applied uniaxial pressure of 400 MPa [7]. All high-temperature operations were carried out under argon. The presence of the ferromagnetic τ -phase was confirmed by X-ray diffraction (XRD) using a Bruker D2 Phaser instrument equipped with a LinxEye linear detector. The magnetic properties of the prepared material were determined in a wide temperature range by a Lake Shore 7400 vibrating sample magnetometer (VSM). A cube-shaped sample of 0.17 g was cut from the sintered compact and mounted in the magnetometer so that its faces were parallel or perpendicular to the applied field.

III. RESULTS

Stable at high temperatures, the hexagonal ϵ -phase can be preserved by quenching and transformed into the tetragonal τ -phase in appropriate heat treatment conditions. An XRD pattern of the sintered sample is shown in Fig. 1. As a result of a composition-invariant structural transition induced by SPS, the ϵ -phase completely disappeared giving rise to the metastable τ -phase. A small amount of the equilibrium β -phase is visible and often correlates with enhanced coercivity

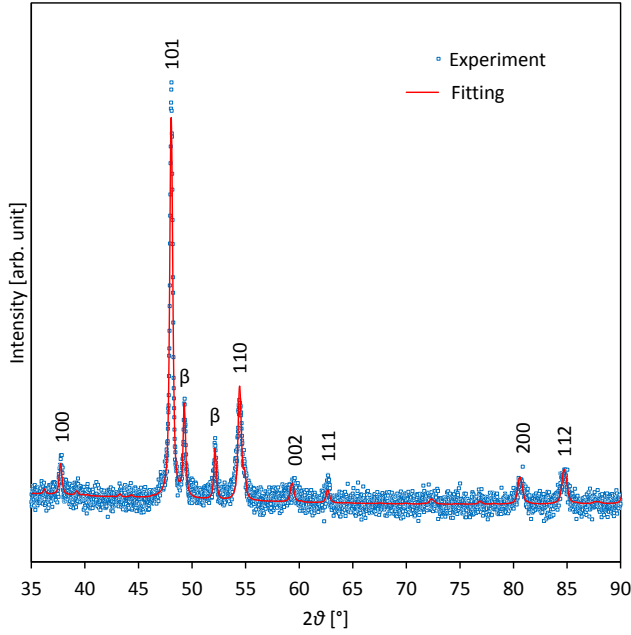


Fig. 1. X-ray diffraction pattern of the sintered $\text{Mn}_{54}\text{Al}_{44}\text{C}_2$ sample (Co $K\alpha$ radiation). The tetragonal τ -phase Miller indices, traces of a secondary β -phase and a Rietveld refinement profile are shown.

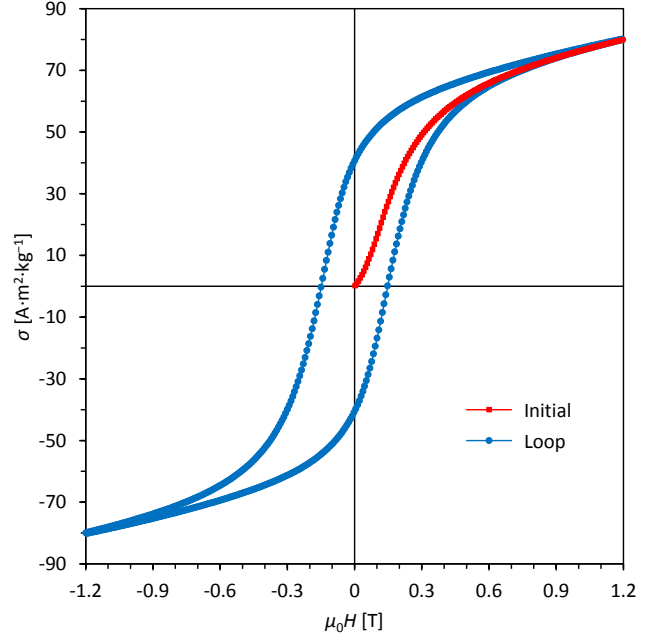


Fig. 2. Initial magnetization curve and hysteresis loop of a heat treated $\text{Mn}_{54}\text{Al}_{44}\text{C}_2$ powder sample at room temperature.

through a pinning mechanism [7]. To estimate the material crystallite size, a Rietveld refinement analysis using MAUD software was performed. No noticeable crystalline texture was detected.

Fig. 2 shows a magnetic hysteresis loop of a heat treated $\text{Mn}_{54}\text{Al}_{44}\text{C}_2$ powder (thermal conditions are similar to those of sintering but no pressure is applied). The initial (virgin) magnetization curve seems to have a characteristic shape indicating that the domain wall pinning is the main mechanism responsible for coercivity.

The observation of magnetic relaxation was carried out as follows. The sample was first fully magnetized, and then the applied field was quickly reversed and kept constant. Under the strong driving force, the metastable states of the domain structure sought to decay. The relaxation mechanisms are generally assumed to rely on thermally activated processes, the relaxation times involved in the experiment are of the order of the measurement characteristic times. The average magnetization M is expected to obey a logarithmic law with respect to time t [10]:

$$M(t) = M(0) - S \ln \left(1 + \frac{t}{t_0} \right), \quad (1)$$

where S is the magnetic viscosity which characterizes the relaxation rate. Equation (1) holds at constant applied field H and temperature T .

The actual experimental curves of the magnetization decay $\Delta M = M(t) - M(0)$ as a function of dimensionless variable $1 + t/t_0$ for different fields H at room temperature are shown in Fig. 3. The empirical constant t_0 is chosen so that to make the dependencies as linear as possible, the adopted value is 1 s (the time for field stabilization of 5 s imposed by the

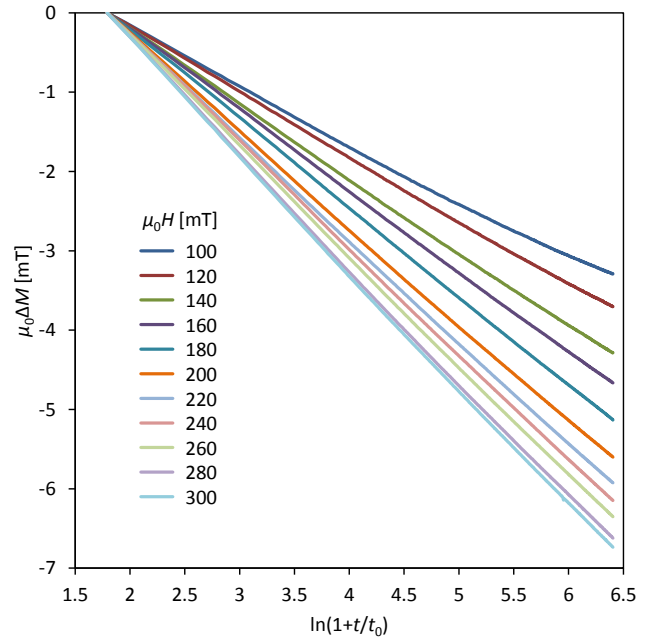


Fig. 3. Magnetization change versus time on a logarithmic scale for different values of the applied field having been reversed (room temperature).

magnetometer is included directly in the experimental data). In agreement with equation (1), the slope of approximating lines determines the magnetic viscosity which exhibits a clear field dependence.

Similar viscosity experiments were performed at various temperatures. Magnetic relaxation retains its logarithmic time behavior in a certain field and temperature range, but accelerates with increase of these variables. Furthermore, magnetiza-

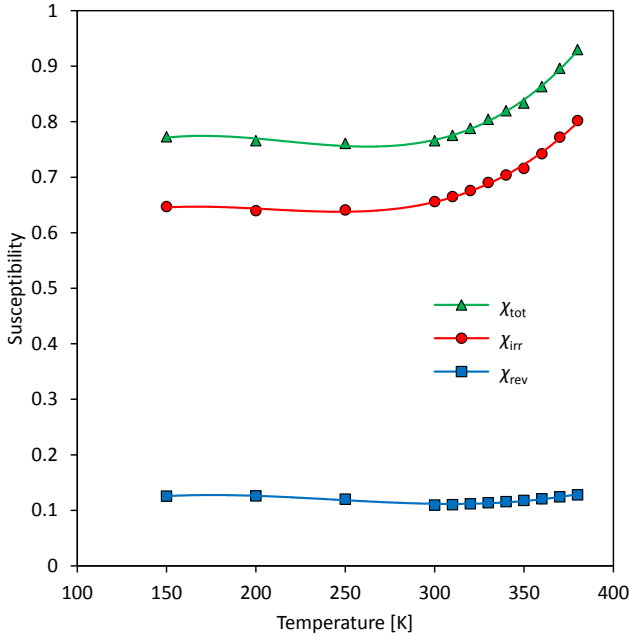


Fig. 4. Reversible (blue), irreversible (red), and total (green) susceptibilities as a function of temperature, measured at near-zero magnetization (data points and third-degree polynomial regression).

tion loops change with temperature. To compare the magnetic viscosity values at different temperatures, each measurement was performed at an applied field equal to the previously determined coercive field, *i.e.* when the mean magnetization is zero.

In order to benefit from the connection between the thermal activation and hysteretic phenomena [11], the total χ_{tot} and reversible χ_{rev} susceptibilities at the major magnetization loop were measured. The irreversible susceptibility $\chi_{\text{irr}} = \chi_{\text{tot}} - \chi_{\text{rev}}$ was then calculated for the applied field at which the corresponding relaxation experiment was performed. These forms of susceptibility are plotted versus temperature in Fig. 4. The reversible susceptibility is small and nearly constant, which helps to simplify the further expressions. The irreversible susceptibility is constant at lower temperatures and shows a relevant thermal dependence at higher temperatures.

Using the irreversible susceptibility χ_{irr} , the magnetic viscosity S can be conveniently expressed in terms of the fluctuation field H_f [12]:

$$S = \chi_{\text{irr}} H_f. \quad (2)$$

The fluctuation field represents a fundamental quantity governing the relaxation process. The average magnetization (1) varies in time as though there was a fictitious field $H_f \ln(1 + t/t_0)$ acting in addition to H on the system. The magnetic viscosity S and fluctuation field H_f as a function of temperature T are shown in Fig. 5. The magnetic viscosity monotonically increases with temperature, whereas the fluctuation field has a maximum slightly above room temperature due to a non-linear temperature dependence of the irreversible susceptibility.

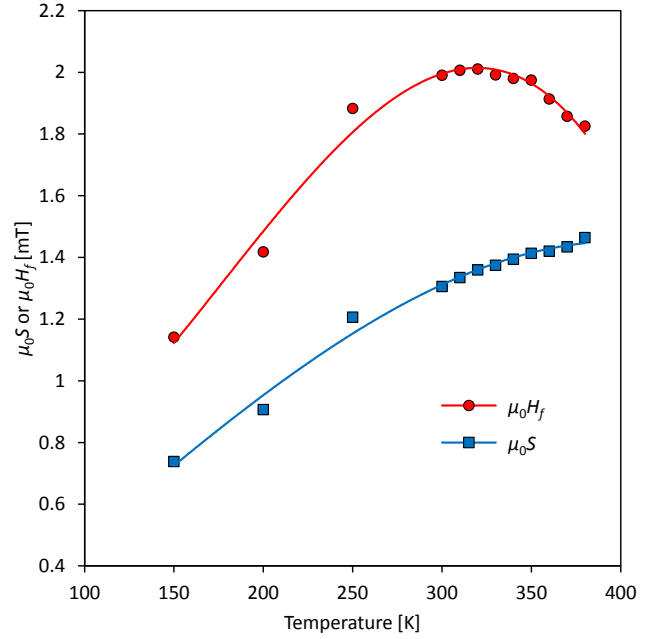


Fig. 5. Temperature dependence of the magnetic viscosity (blue) and fluctuation field (red) derived from the relaxation and susceptibility measurements (data points and third-degree polynomial regression).

The fluctuation field H_f is related to the activation volume v , a typical volume involved in a single relaxation event [10]:

$$v = \frac{k_B T}{\mu_0 M_s H_f}. \quad (3)$$

Here k_B is Boltzmann constant and M_s is the saturation magnetization estimated from high-field measurements [13]. As shown in Fig. 6, the activation volume v sharply increases with temperature having a value of $4 \cdot 10^{-24} \text{ m}^{-3}$ at 300 K. A similar temperature dependence of the activation volume is observed, for example, in Nd-Fe-B magnets [14], [15].

Nucleation of reversed domains can be analyzed from a general viewpoint of energy balance. In this phenomenological model the coercive field H_c is interpreted as the value of applied field for which the formation of a nucleus of volume v becomes energetically favored, which gives [10]:

$$H_c = \alpha \frac{\gamma_w}{\mu_0 M_s v^{1/3}} - N_{\text{eff}} M_s. \quad (4)$$

Here α and N_{eff} are dimensionless parameters measuring how far the material is from the ideal conditions and representing the relative importance of magnetocrystalline anisotropy and dipolar interactions, respectively [14], [15]. The domain wall energy (surface tension) γ_w is estimated as usually:

$$\gamma_w = 4\sqrt{AK_1}, \quad (5)$$

where A is the exchange constant and K_1 is the uniaxial anisotropy constant. The values of these parameters (and the temperature dependence) were taken from literature [13], [16]. The wall energy γ_w is plotted versus temperature in Fig. 6 together with the activation volume v .

When magnetization reversal is thermally activated, the reversed nucleus is formed by the same processes that are

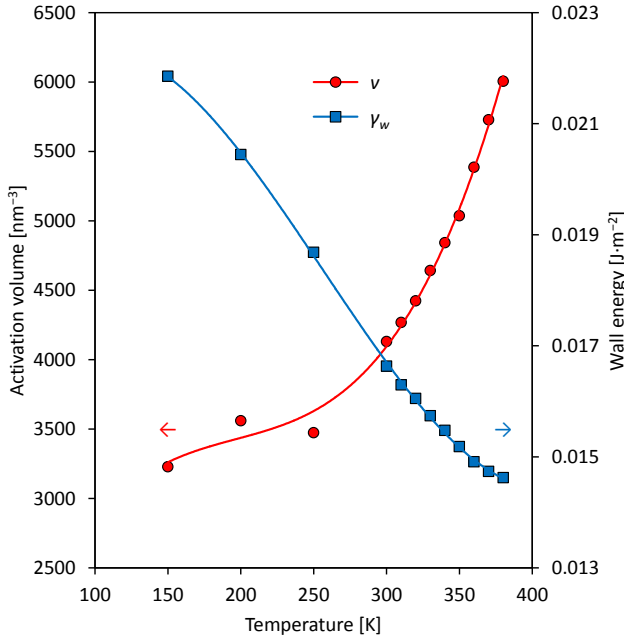


Fig. 6. Experimental activation volume (red) and calculated domain wall energy (blue) as a function of temperature (data points and third-degree polynomial regression).

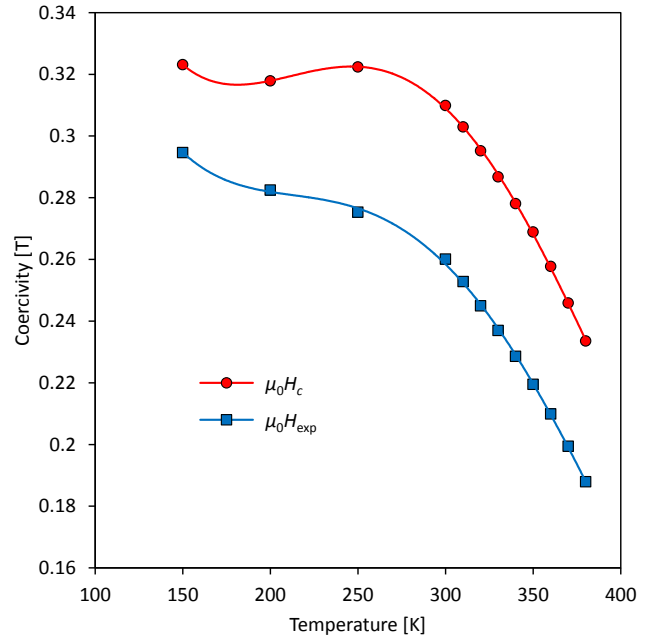


Fig. 7. Measured coercive field (blue) and the coercivity corrected for the fluctuation field (red) as a function of temperature (data points and fourth-degree polynomial regression).

responsible for magnetic viscosity. This means that the critical volume v can be estimated from the magnetic viscosity experiment. Assuming that energy barriers of height up to $25k_B T$ are overcome by thermal activation in usual measurement time, one can write the following relation [10]:

$$H_c = H_{\text{exp}} + 25H_f. \quad (6)$$

Here H_c is the intrinsic coercive field, purged of thermal relaxation effects, which is to be used in the analysis, and H_{exp} is the experimental coercive field. In Fig. 7 these fields are plotted versus temperature. The measured field H_{exp} monotonically decreases with temperature, whereas the intrinsic field H_c reaches a plateau at low temperatures caused by a decrease of the fluctuation field (*cf.* Fig. 5).

The parameters α and N_{eff} are assumed constant for a given material. One can present equation (4) in a dimensionless form dividing both sides by M_s . In order to verify the validity of the underlying model, the reduced nucleus energy $\gamma_w/(\mu_0 M_s^2 v^{1/3})$ was plotted versus the reduced coercive field H_c/M_s at different temperatures in Fig. 8, where the coercivity is redefined according to equation (6).

The phenomenological parameters of the magnetization reversal model determined from linear regression are $\alpha = 0.19$ and $N_{\text{eff}} = 0.13$. One can see that relation (4) describes the material particularly well in the temperature interval of 300 to 360 K (red circles in Fig. 8). At higher temperatures (yellow triangles) a departure from the linear trend is noticeable, which may be partially related to the observed deviation from the logarithmic law in the viscosity experiments. At lower temperatures (blue squares) the dependence completely changes: the coercive field H_c is practically constant, whereas

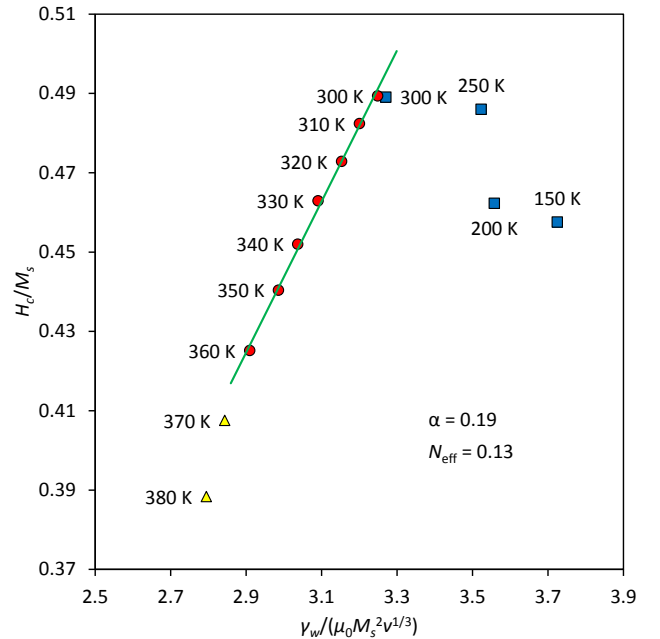


Fig. 8. Relation between the reduced coercive field H_c/M_s and the reduced nucleus energy $\gamma_w/(\mu_0 M_s^2 v^{1/3})$ at different temperatures. A linear trend line with fitting parameters are shown.

the saturation magnetization M_s continues to increase when temperature decreases.

IV. DISCUSSION

Equations (4) and (6) describe a thermally activated process of the reverse domain nucleation. In this case a correlation

between the activation length $v^{1/3}$ and the domain wall thickness

$$\delta_w = \pi \sqrt{\frac{A}{K_1}}, \quad (7)$$

is often observed. Indeed, according to our data, both quantities are of the same order of magnitude and show similar temperature dependence. Typical values are $v^{1/3} = 16$ nm and $\delta_w = 12$ nm at 300 K (as a rule, $v^{1/3} > \delta_w$).

Another possibility is athermal formation of the reverse nucleus. In this case the role of critical volume is played by the whole grain, and equation (4) holds with $v^{1/3} = d$, where d is the average grain size. Besides, the coercivity correction (6) seems to be unnecessary. The size of coherently scattering crystallites is estimated as 60 nm from XRD. It is worth noting that this characteristic is usually smaller than the average grain size because of the presence of defects. The ferromagnetic τ -phase in Mn–Al–C alloys is the result of a structural phase transition [17] and is known to contain regular planar defects such as twins, stacking faults and antiphase boundaries [18], [19]. On the other hand, the magnetic domain structure may interact with the lattice defects, so that the d value can be smaller than the grain size.

Fig. 8 shows that the coercivity drops from the linear trend at lower temperatures. As an alternative interpretation we might assume a critical volume for these points larger than the activation volume determined from the magnetic relaxation measurements, suggesting a contribution from the athermal mechanism of reverse domain nucleation. As for the points on the line, a typical value of dimensionless variable $\gamma_w/(\mu_0 M_s^2 v^{1/3})$ is only twice as lower as the reduced anisotropy field $2K_1/M_s^2$. Therefore, the main problem for this system remains a small value of the slope α .

V. CONCLUSION

Magnetic viscosity, fluctuation field and activation volume were measured in a $\text{Mn}_{54}\text{Al}_{44}\text{C}_2$ permanent magnet in a range of temperatures. These data were used to analyze the magnetization reversal and temperature dependence of the coercive field. The thermally activated mechanism of the reversed nucleus formation was confirmed, with possible contribution from an athermal process. The role of magnetic and structural characteristic lengths was discussed.

ACKNOWLEDGMENT

The spark plasma sintering was performed at the Plateforme de Frittage Ile de France (Thiais, France).

REFERENCES

- [1] J. M. D. Coey, "Permanent magnets: Plugging the gap," *Scr. Mater.*, vol. 67, pp. 524–529, Sep. 2012.
- [2] M. J. Kramer, R. W. McCallum, I. A. Anderson, and S. Constantinides, "Prospects for non-rare earth permanent magnets for traction motors and generators," *JOM*, vol. 64, pp. 752–763, Jul. 2012.
- [3] J. Cui, M. Kramer, L. Zhou, F. Liu, A. Gabay, G. Hadjipanayis, B. Balasubramanian, and D. Sellmyer, "Current progress and future challenges in rare-earth-free permanent magnets," *Acta Mater.*, vol. 158, pp. 118–137, Oct. 2018.
- [4] H. Kono, "On the ferromagnetic phase in manganese-aluminum system," *J. Phys. Soc. Jpn.*, vol. 13, pp. 1444–1451, Dec. 1958.

- [5] A. J. J. Koch, P. Hokkeling, M. G. van der Steeg, and K. J. de Vos, "New material for permanent magnets on a base of Mn and Al," *J. Appl. Phys.*, vol. 31, pp. S75–S77, May 1960.
- [6] T. Ohtani, N. Kato, S. Kojima, K. Kojima, Y. Sakamoto, I. Konno, M. Tsukahara, and T. Kubo, "Magnetic properties of Mn–Al–C permanent magnet alloys," *IEEE Trans. Magn.*, vol. 13, pp. 1328–1330, Sep. 1977.
- [7] A. Pasko, M. LoBue, E. Fazakas, L. K. Varga, and F. Mazaleyrat, "Spark plasma sintering of Mn–Al–C hard magnets," *J. Phys. Condens. Matter*, vol. 26, p. 064203, Feb. 2014.
- [8] R. Madugundo and G. C. Hadjipanayis, "Anisotropic Mn–Al–(C) hot-deformed bulk magnets," *J. Appl. Phys.*, vol. 119, p. 013904, Jan. 2016.
- [9] M. Tyrman, S. Quétel-Weben, A. Pasko, L. Perrière, I. Guillot, V. Etgens, and F. Mazaleyrat, "Ferromagnetic L_{10} phase formation in the Mn–Al–C alloys induced by high-pressure spark plasma sintering," *IEEE Trans. Magn.*, vol. 53, p. 2101505, Nov. 2017.
- [10] G. Bertotti, *Hysteresis in Magnetism*. San Diego: Academic Press, 1998.
- [11] V. Basso, B. Cinzia, M. LoBue, P. Tiberto, and G. Bertotti, "Connection between hysteresis and thermal relaxation in magnetic materials," *Phys. Rev. B*, vol. 61, pp. 1278–1285, Jan. 2000.
- [12] E. P. Wohlfarth, "The coefficient of magnetic viscosity," *J. Phys. F*, vol. 14, pp. L155–L159, Aug. 1984.
- [13] A. Pasko, F. Mazaleyrat, L. K. Varga, P. Stamenov, and J. M. D. Coey, "High-field magnetization behavior of Mn–Al–C alloys," *IEEE Trans. Magn.*, vol. 50, p. 2105104, Nov. 2014.
- [14] D. Givord, Q. Lu, M. F. Rossignol, P. Tenaud, and T. Viadieu, "Experimental approach to coercivity analysis in hard magnetic materials," *J. Magn. Magn. Mater.*, vol. 83, pp. 183–188, Jan. 1990.
- [15] D. W. Taylor, V. Villas-Boas, Q. Lu, M. F. Rossignol, F. P. Missell, D. Givord, and S. Hirosawa, "Coercivity analysis in $\text{R}_{17}\text{Fe}_{23-x}\text{B}_x$ magnets," *J. Magn. Magn. Mater.*, vol. 130, pp. 225–236, Feb. 1994.
- [16] Moreno, "Temperature-dependent exchange stiffness and domain wall width in Co," *Phys. Rev. B*, vol. 94, p. 104433, Sep. 2016.
- [17] S. Kojima, T. Ohtani, N. Kato, K. Kojima, Y. Sakamoto, I. Konno, M. Tsukahara, and T. Kubo, "Crystal transformation and orientation of Mn–Al–C hard magnetic alloy," *AIP Conf. Proc.*, vol. 24, pp. 768–769, Jan. 1975.
- [18] J. J. Van Den Broek, H. Donkersloot, G. Van Tendeloo, and J. Van Landuyt, "Phase transformations in pure and carbon-doped $\text{Al}_{45}\text{Mn}_{55}$ alloys," *Acta Metall.*, vol. 27, pp. 1497–1504, Sep. 1979.
- [19] J. M. K. Wiezorek, A. K. Kulovits, C. Yanar, and W. A. Soffa, "Grain boundary mediated displacive–diffusional formation of τ -phase MnAl," *Metall. Mater. Trans. A*, vol. 42, pp. 594–604, Mar. 2011.